

Topical Review

Methods for modeling cytoskeletal and DNA filaments

Steven S Andrews

Division of Basic Sciences, Fred Hutchinson Cancer Research Center, 1100 Fairview Avenue North, Seattle, WA 98109, USA

E-mail: sandrews@fhcrc.org

Received 18 March 2013, revised 3 November 2013

Accepted for publication 12 December 2013

Published 29 January 2014

Abstract

This review summarizes the models that researchers use to represent the conformations and dynamics of cytoskeletal and DNA filaments. It focuses on models that address individual filaments in continuous space. Conformation models include the freely jointed, Gaussian, angle-biased chain (ABC), and wormlike chain (WLC) models, of which the first three bend at discrete joints and the last bends continuously. Predictions from the WLC model generally agree well with experiment. Dynamics models include the Rouse, Zimm, stiff rod, dynamic WLC, and reptation models, of which the first four apply to isolated filaments and the last to entangled filaments. Experiments show that the dynamic WLC and reptation models are most accurate. They also show that biological filaments typically experience strong hydrodynamic coupling and/or constrained motion. Computer simulation methods that address filament dynamics typically compute filament segment velocities from local forces using the Langevin equation and then integrate these velocities with explicit or implicit methods; the former are more versatile and the latter are more efficient. Much remains to be discovered in biological filament modeling. In particular, filament dynamics in living cells are not well understood, and current computational methods are too slow and not sufficiently versatile. Although primarily a review, this paper also presents new statistical calculations for the ABC and WLC models. Additionally, it corrects several discrepancies in the literature about bending and torsional persistence length definitions, and their relations to flexural and torsional rigidities.

Keywords: cytoskeleton, DNA, filament mechanics, filament dynamics, polymer theory

Nomenclature

Abbreviations

ABC	angle-biased chain model
FJC	freely jointed chain model
GC	Gaussian chain model
WLC	wormlike chain model

Roman symbols

A_j	direction cosine matrix for j th segment
-------	--

 Content from this work may be used under the terms of the [Creative Commons Attribution 3.0 licence](https://creativecommons.org/licenses/by/3.0/). Any further distribution of this work must maintain attribution to the author(s) and the title of the work, journal citation and DOI.

a	effective reptation tube segment length
$a_{\chi,j}$	bending or twisting angle of joint j on axis χ
a_{χ}°	intrinsic bending or twisting angle on axis χ
b	segment length
b_{Kuhn}	Kuhn length
$C_n, C(s)$	bending autocorrelation function
$C_{\text{tor},n}, C_{\text{tor}}(s)$	torsional autocorrelation function
D	filament diffusion coefficient
E	Young's modulus
E_j	bending or stretching potential energy of segment j
\mathbf{e}_d	unit vector parallel to Cartesian axis d
F	elastic force
\mathbf{f}	random thermal force

G	shear modulus
I_χ	area moment of inertia on axis χ
J	torsional constant
k_B	Boltzmann's constant
k_χ	bending or twisting force constant on axis χ
L	total filament contour length
$\mathcal{L}(\dots)$	Langevin function
N	number of filament segments
P	bending persistence length
$P_{\text{tor.}}$	torsional persistence length
\mathbf{R}	filament end-to-end vector
\mathbf{r}_j	endpoint of segment j
r	bead or filament radius
s	contour length coordinate along a filament
T	temperature in Kelvin
$X_n, X(s)$	bending cross-correlation function
$X_{\text{tor.},n}, X_{\text{tor.}}(s)$	torsional cross-correlation function
x	separation between filament ends

Greek symbols

$\alpha_\chi(s)$	curvature at contour length s on axis χ
α_χ°	intrinsic curvature on axis χ
$\varepsilon(s)$	bending energy density at contour length s
ζ	hydrodynamic friction coefficient
η	solvent viscosity
κ	flexural rigidity of rotationally symmetric filament
κ_χ	flexural ($\chi = \theta$ or ϕ) or torsional ($\chi = \psi$) rigidity
ν	Poisson's ratio
σ_χ	standard deviation of rotation on axis χ
τ	slowest time constant for filament relaxation

Subscripts

j	index for filament segments or joints
R	Rouse model
rept.	reptation model
rod	stiff rod model
tor.	torsional
Z	Zimm model
θ	pitch axis (bending down or up)
ϕ	yaw axis (bending left or right)
χ	index for θ , ϕ , or ψ
ψ	roll axis (twisting counter-clockwise or clockwise)

1. Introduction

Nearly all biological cells rely on both cytoskeletal and DNA filaments to carry out essential cellular functions. Cytoskeletal filaments create cell structure, drive cell motility, arrange chromosomes during cell division, and serve as tracks for cellular cargo transport, among other tasks. DNA encodes the cell's genetic information and makes it available for replication and transcription. Both classes of filaments are highly dynamic. They are assembled and disassembled. They also bend, exert forces on membranes, and interact specifically with numerous proteins. One way to investigate the biophysics

that underlie these dynamics is through quantitative filament modeling, whether with analytical equations or computer simulations.

This review surveys the models that researchers use to represent biological filament mechanics and dynamics. It focuses particularly on simple mechanical models that represent individual filaments in continuous space. It addresses cytoskeletal and DNA filaments together, despite their very different cellular roles, because they share many mechanical properties and because the research on these two filament classes is complementary. Research on filament networks [1–5], lattice models [6–8], and RNA [9] and protein [10] folding has also led to many interesting results but is outside of the scope of this review.

Filament models can be classified by whether they address filament conformations, which focus on filaments in equilibrium, or filament dynamics, which focus on filaments in motion. As described below, conformational models include the freely jointed chain (FJC), Gaussian chain (GC), angle-biased chain (ABC), and wormlike chain (WLC) models. In all of these cases, the model definition defines the filament bending and stretching energies. Filament entropies can be computed from these energies, assuming statistical ensembles of filaments. Then, average conformations and elasticities derive from the energies and entropies. Dynamical models include the Rouse, Zimm, stiff rod, dynamic WLC, and reptation models. These model definitions define the forces on each filament, such as from filament bending rigidities, Brownian motion, and hydrodynamic interactions. Filament diffusion coefficients and relaxation times derive from these forces. Computational methods complement these analytical models by being able to represent much more complexity, but at the cost of only evaluating models with a single set of parameter values at a time.

2. Cytoskeletal and DNA filaments

There are three main types of eukaryotic cytoskeletal filaments [11, 12] (table 1). (i) *Actin filaments*, made of actin protein, are most concentrated close to the plasma membrane. They help determine cell surface shape, produce cell motility, and form the structures of small cell protrusions such as stereocilia and microvilli [13, 14]. Together with myosin motors, they form the primary contractile apparatus of muscle cells. (ii) *Microtubules* are long hollow stiff cylinders of tubulin protein [15, 16]. They determine the positions of membrane-enclosed organelles and direct intracellular transport, including of the chromosomes during mitosis. They also provide structural support to cells, including to cilia and flagella. And (iii) *intermediate filaments* are a diverse class of flexible filaments that provide mechanical strength to cells [17]. They make up hair, nail, horn, and scale cells, they form the nuclear lamina, which lies just inside the inner nuclear membrane, they span cells to provide strength to epithelial tissues, and they anchor organelles and stabilize the cytoplasm.

Bacterial cytoskeletons differ substantially from eukaryotic ones [18, 19]. However, they include structurally homologous proteins in each of the three major classes.

Table 1. Mechanical properties of DNA and eukaryotic cytoskeletal filaments. Polarity refers to the equivalence of the filament ends, where ‘np’ indicates not polar and ‘p’ indicates polar. Persistence lengths are from published experimental results (except for microtubule torsion, which is from a published model [78]). Where publications only listed flexural or torsional rigidities, I computed persistence lengths for 25 °C using equations (15) and (17). Question marks indicate unmeasured quantities. However, the intermediate filament torsional persistence length can likely be estimated from equation (24).

Eukaryotic filament	Strands, polarity	Outer diameter	Bending persistence length	Torsional persistence length	Breaking strength	Bacterial homologs	References
DNA	2, np	2.4 nm	45–50 nm	140 nm	0.48 nN	DNA	[32, 35, 137, 138]
Actin	2, p	5–9 nm	16–18 μ m	39 μ m	0.6 nN	MreB, Mbl, ParM	[11, 37, 61, 105, 139, 140]
Microtubules	~13, p	25 nm	2–6 mm	0.5 mm	?	FtsZ, TubZ	[27, 38, 62, 78, 141–143]
Intermediate filaments	6–10, np	~10 nm	~1 μ m	?	1–2 nN	croscentin	[12, 17, 28, 63, 144]

There are as many as 35 actin-like bacterial protein families [20], of which MreB and ParM are particularly well studied and likely to be particularly important [21, 22]. MreB helps determine cell shape while ParM helps segregate plasmids in preparation for cell division [19]. The tubulin homolog FtsZ is widespread in bacteria, archaea and some intracellular eukaryotic organelles [23, 24]. It forms the so-called Z-ring at the cell division site that likely constricts to divide the cell [25–27]. Finally, the *Caulobacter crescentus* crescentin protein is an intermediate filament structural homolog [28]. It forms a filament bundle along the inside of the cell membrane, parallel to the cell’s long axis, where it appears to resist elongation forces from cell growth and hence induces cell curvature. Bacteria also express several cytoskeletal proteins that do not have eukaryotic counterparts [19]. These include the *Spiroplasma* Fib protein, which assembles into a flattened ribbon and acts as a linear motor [29], the plasmid-encoded ParA protein, which helps segregate plasmids during cell division [30], and the *Escherichia coli* MinD protein, which oscillates between the cell poles to help center the cell division plane [31].

DNA encodes each cell’s genetic information. It has antiparallel strands and is nearly always double stranded. The DNA double helix can adopt A, B, or Z forms, which have different diameters and different helical pitches (additionally, the A and B forms are right-handed, while the Z form is left-handed). The B form is most common under cellular conditions and is the focus of most research on DNA mechanics [32]. Where this review discusses DNA, it refers to the B form of double stranded DNA. Eukaryotic cells package DNA with several levels of organization [33]. DNA wraps around histones to form the ‘beads on a string’ form of chromatin; this gets folded into a compact chromatin fiber, and the chromatin fiber is packed into higher order structures, such as a metaphase chromosome, in the cell’s nucleus [34].

All of these filaments have many things in common. Each comprises multiple strands, or proto-filaments, that wrap around each other in helices. In some cases, including actin and microtubules, the strands are oriented in the same direction which gives the filament an overall polarity. In other cases, including DNA and intermediate filaments, the strands are oriented in opposite directions which makes the two filament ends essentially equivalent (not accounting for DNA sequences, which are typically asymmetric). For each filament class, table 1 lists the filament diameters and *persistence*

lengths. Qualitatively, a filament’s persistence length is its stiffness; it is the length along the filament’s contour where thermal bending or twisting influences become substantial. Quantitatively, the persistence length is typically defined as the statistical correlation length for the relative filament orientations at two points along the filament [12, 35–37] (see sections 3.3 and 3.5 for details). Persistence lengths vary greatly between different biological filament types, which gives them very different structural behaviors within cells. For example, persistence lengths range from 50 nm for DNA [35] to about 2 mm for microtubules [38]. This means that DNA is flexible enough to easily fold into compact structures within nuclei, whereas microtubules are so stiff that they exhibit minimal thermal bending across entire cells (microtubules primarily bend in response to forces induced by motor proteins). For all filaments considered here, their diameters are much smaller than their persistence lengths, which enables them to be treated mechanically as ‘thin’ filaments [39].

3. Filament conformations

Biological filament modeling builds on a long history of polymer theory, which many excellent texts cover in detail. These include [12, 40–44]. This section repeats some of the central results, focusing on their relevance to biological filaments.

The conformational models considered in this section treat filaments as thin rods that bend either at joints or continuously along their contours (figure 1). These treatments assume a sufficiently coarse level of detail that microscopic filament details, such as specific chemical moieties, can be neglected. They also assume that filaments are sufficiently thin, electrically neutral, and well solvated that *long-range interactions* between different filament regions can be ignored. *Short-range interactions* are between regions that are reasonably close along the filament’s contour, while long-range interactions are between regions that are widely separated along the filament’s contour, even if they are physically proximate due to filament bending. The assumption of good solvation is equivalent to assuming that filament-solvent contact is energetically equivalent to filament–filament contact. As a contrasting example, unfolded proteins generally cannot be considered to be well solvated because they have hydrophobic residues that are energetically driven to associate with each other rather than with the aqueous medium of

Table 2. Statistical properties of filament conformation models. The models and statistical properties are defined in the main text. Persistence lengths are undefined in the FJC and GC models, so are shown as not applicable (N/A). The elasticity has not been computed for the ABC model, so is represented with a ‘?’. Literature references for the FJC, GC, and WLC equations are in the main text. The [appendix](#) shows derivations for the ABC model.

	Freely jointed chain (FJC)	Gaussian chain (GC)	Angle-biased chain (ABC)	Wormlike chain (WLC)
Bending persistence length, P	N/A	N/A	$\frac{2bk_\theta k_\phi}{k_B T(k_\theta + k_\phi)}$	$\frac{2\kappa_\theta \kappa_\phi}{k_B T(\kappa_\theta + \kappa_\phi)}$
Torsional persistence length, P_{tor}	N/A	N/A	$\frac{2bk_\psi}{k_B T}$	$\frac{2\kappa_\psi}{k_B T}$
Kuhn length, b_{Kuhn}	b	b	$b \coth \frac{b}{2P}$	$2P$
Ms end-to-end distance, $\langle \mathbf{R}^2 \rangle$	bL	bL	$\frac{Lb \sinh \frac{b}{P} - b^2(1 - e^{-L/P})}{\cosh \frac{b}{P} - 1}$	$2LP - 2P^2(1 - e^{-L/P})$
Elasticity, F	$\frac{k_B T}{b} \mathcal{L}^{-1} \left(\frac{x}{L} \right)$	$\frac{3k_B T x}{bL}$?	small x : $\frac{3k_B T x}{2PL}$; large x : $\sim \frac{k_B T}{P} \left[\frac{1}{4} \left(1 - \frac{x}{L} \right)^{-2} - \frac{1}{4} + \frac{x}{L} \right]$

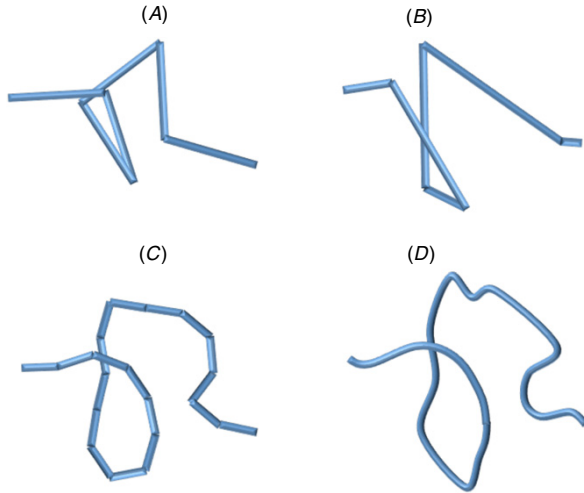


Figure 1. Filament conformation models. These models are described in the main text. (A) Freely jointed chain (FJC), (B) Gaussian chain (GC), (C) angle-biased chain (ABC), (D) wormlike chain (WLC).

the cytoplasm; this is the reason why protein and RNA folding are outside of the scope of this review. The assumptions listed here are often valid for DNA and cytoskeletal filaments, as seen by that fact that good agreement is typically observed between experimental and model results, as described below.

3.1. Freely jointed and Gaussian chain models

The *FJC* model (figure 1(A)), also called the random flight model, is a conceptually important filament model that was introduced independently by Kuhn [45] and Guth and Mark [46] in 1934. It represents a filament as a sequence of N straight segments that are joined together with unconstrained random

angles. The length of each segment, b , is called the *Kuhn length*.

Several model statistics are useful (table 2). First, the total *contour length*, L , is the length of the fully extended filament and is simply

$$L = Nb. \quad (1)$$

Filaments are typically not fully extended though, so it is helpful to consider the vector that points from one end of the filament to the other, denoted \mathbf{R} (this follows convention by defining \mathbf{R} as the end-to-end vector, but the following statistics also apply to any two filament points that are separated by N segments or L contour length). The average value of \mathbf{R} , considering the entire ensemble of conformations that a filament could adopt in unconstrained space, equals 0 because the filament as a whole is equally likely to have any orientation. More usefully, the average separation between the ends is the *root mean squared (rms) end-to-end distance*, which is [41]

$$\langle \mathbf{R}^2 \rangle^{1/2} = b\sqrt{N} = \sqrt{bL}, \quad (2)$$

where the angle brackets denote the average over all conformations. (This is easily verified for a filament on a lattice: adding a single segment to an existing chain, with equal probability for each direction, increases $\langle \mathbf{R}^2 \rangle$ by b^2 .) Notably, this measure of the filament size grows with the square root of the filament’s contour length. This is because random filaments tend to collapse into loose clusters rather than extended conformations due to the former’s greater entropy. The full distribution of this end-to-end vector gives more detail but the same qualitative result; it approaches the following Gaussian distribution as the number of segments increases [41],

$$\Phi(\mathbf{R}, N) = \left(\frac{3}{2\pi Nb^2} \right)^{3/2} \exp \left(-\frac{3\mathbf{R}^2}{2Nb^2} \right). \quad (3)$$

The standard deviation of this Gaussian is $(bL/3)^{1/2}$, which again grows as the square root of the contour length. Yet another standard measure of a filament’s size is the *radius*

of gyration, which is the rms filament radius, now considering all parts of the filament rather than just the ends, and taken relative to the filament's center of mass. It is $(bL/6)^{1/2}$ [41]. Yet again, the linear extent of a random filament grows as the square root of the contour length.

This tendency of a filament to collapse into a loose cluster is responsible for the counterintuitive result that random filaments exert a mechanical force against stretching, despite the fact that all the joints in the FJC model are completely unconstrained. This *entropic elasticity*, which arises only from the decrease in configurational entropy that occurs when a filament is stretched, is

$$F = \frac{3k_B T}{bL} x \quad (4)$$

for small displacements [12]. Here, x is the separation of the two filament ends, k_B is Boltzmann's constant and T is the absolute temperature. In other words, a FJC acts as an ideal spring with spring constant $3k_B T/bL$. The exact force–extension relationship, now allowing for large displacements as well as small ones, is [44]

$$x = L\mathcal{L}\left(\frac{Fb}{k_B T}\right), \quad (5)$$

where $\mathcal{L}(\dots)$ is the Langevin function, defined as

$$\mathcal{L}(a) = \coth a - \frac{1}{a}. \quad (6)$$

(The Langevin function should not be confused with the total contour length, despite the fact that both are represented by the letter L .) According to this equation, a filament's elastic force grows linearly with the displacement at first, but then grows faster and approaches infinity as the displacement approaches the contour length (figure 2).

The *GC model* (figure 1(B)) replaces the fixed length segments of the FJC model with Gaussian-distributed random length segments that have average (rms) length b . This assumption is accomplished by positing a segment stretching energy [41],

$$E_j = \frac{3k_B T}{2b^2} (\mathbf{r}_j - \mathbf{r}_{j-1})^2, \quad (7)$$

where E_j is the stretching energy of segment j and \mathbf{r}_j is the position of the end of segment j . This means that each segment is an ideal spring with spring constant $3k_B T/b^2$ —the same spring constant as for small displacements of the FJC model (equation (4)). This segment elasticity gives the GC model convenient theoretical properties. It has the same rms end-to-end length (equation (2)) and radius of gyration as the FJC, but now the end-to-end vector distribution is exactly Gaussian (equation (3)) and the elasticity is exactly linear (equation (4)), independent of chain length. Furthermore, these statistics are conserved even if the chain is treated at a different level of resolution, ranging from just a single segment for the whole chain to a continuum of segments [41]. On the other hand, figure 2 shows that the GC model elasticity agrees less well with experiment than does the FJC model.

The FJC and GC models are important, despite their severe approximations of straight segments and unconstrained joints, because they are simple enough to be convenient and to lend physical insight, while still being accurate enough

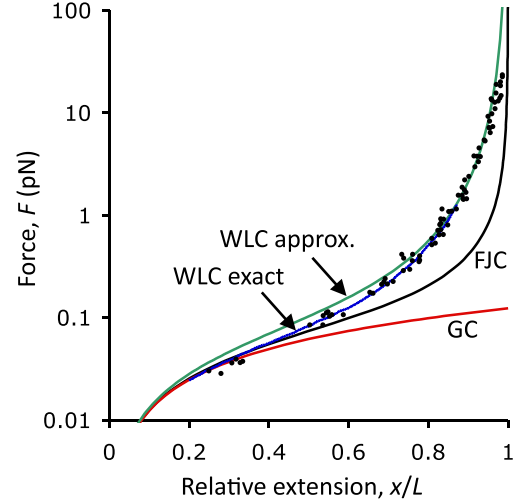


Figure 2. Elasticity of different filament conformation models. The black line represents the freely jointed chain model (equation (5)), the red line represents the Gaussian chain model (equation (4)), the blue line represents the exact solution for the wormlike chain model (from [48]), and the green line represents an approximate solution for the wormlike chain model (equation (14)). Black points represent Bustamante *et al*'s experimental DNA force-extension data [48], which are republished with permission. Model parameters are 50 nm persistence lengths and 100 nm Kuhn lengths.

that many of their qualitative behaviors agree reasonably well with experiment. For example, Smith and coworkers [47] found that the radius of gyration of double stranded DNA grows in proportion to the contour length to the 3/5 power, which is close to the 1/2 power predicted by these models (the difference arises from the filament's excluded volume [41, 47]). Also, figure 2 shows that the FJC elasticity relationship agrees qualitatively (but not quantitatively) with that for DNA measurements [48]; both are linear for small displacements and become steeper for larger displacements. Furthermore, the filament conformation statistics quoted above are not limited to these two models, but apply quite generally to all filament models that treat suitably long filaments and that ignore long-range interactions [41].

3.2. Angle-biased chain model

Removing the FJC model assumption of unconstrained joints leads to what I call the ABC model (figure 1(C)). This model accounts for short-range interactions, such as steric interactions between sequential segments, by positing bending energies that bias the joint angles between segments toward small values. For a filament in three-dimensional space, each bending energy is [49]

$$E_j = \frac{k_\phi}{2} (a_{\phi,j} - a_\phi^\circ)^2 + \frac{k_\theta}{2} (a_{\theta,j} - a_\theta^\circ)^2 + \frac{k_\psi}{2} (a_{\psi,j} - a_\psi^\circ)^2. \quad (8)$$

The three terms represent the three rotational degrees of freedom. Most authors (e.g. [36, 50–53]) represent them with *Euler angles*. Here, one envisions oneself facing ‘forwards’ along a filament (e.g. toward the ‘plus’ end for actin or

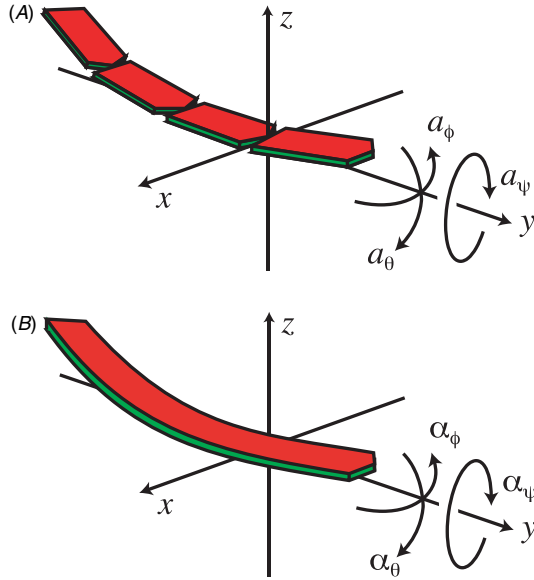


Figure 3. Tait–Bryan rotational angles for (A) the angle-biased chain model and (B) the wormlike chain model. Subscripts are ϕ for yaw, θ for pitch, and ψ for roll; the first two are transverse angles and the last is a torsional angle. Arrows point in the direction of positive rotation. Reprinted with permission from [49]. Copyright 2007 Elsevier.

microtubules); then, the θ angle represents bending away from the straight-ahead line, the ϕ angle represents the azimuth of the bend, and the ψ angle represents filament twisting. Euler angles represent simple chemical polymers naturally because these filaments often have reasonably fixed bending angles and reasonably free twisting rotations (the polyethylene backbone, for example, is linked with single chemical bonds that have 112° bond angles; here, $\theta = 68^\circ$ and ϕ varies from 0° to 360°). The *Tait–Bryan angles* [49, 54], commonly used for ships and airplanes, are an alternate coordinate system (figure 3). In this convention, one again envisions oneself facing forwards along the filament; then, the ϕ angle represents bending toward the left or right, called yaw, the θ angle represents bending down or up, called pitch, and the ψ angle represents twisting counter-clockwise or clockwise, called roll. For example, each base pair of unbent DNA has 0 yaw angle, 0 pitch angle, and 34° of roll angle. Tait–Bryan angles are generally more convenient than Euler angles for filaments that have restricted twisting rotations, which includes all filaments considered here. For example, they represent rotationally asymmetric filaments naturally; examples include cytoskeletal filaments that have membrane-binding faces, such as MreB [49]. For these reasons, this review uses Tait–Bryan angles. Returning to equation (8), $a_{\phi,j}$, $a_{\theta,j}$ and $a_{\psi,j}$ are the yaw, pitch and roll angles for the j th joint, a_ϕ° , a_θ° and a_ψ° are the *intrinsic* or *preferred angles*, which characterize the intrinsic filament curvature and twisting, and k_ϕ , k_θ and k_ψ are the spring force constants, assuming harmonic springs. For rotationally symmetric filaments, the a_ϕ° and a_θ° values equal zero and the k_ϕ and k_θ force constants equal each other [35]. Filaments in two dimensions, such as cytoskeletal filaments bound to

planar membranes, can only bend toward the left or right at each joint so the two-dimensional version of equation (8) only has a single term: $k_\phi(a_{\phi,j} - a_\phi^\circ)^2/2$ [55].

The Boltzmann distribution gives the rotation angle equilibrium distribution for the ABC model [55],

$$p(a_{\chi,j}) = \sqrt{\frac{k_\chi}{2\pi k_B T}} \exp\left(-\frac{k_\chi (a_{\chi,j} - a_\chi^\circ)^2}{2k_B T}\right), \quad (9)$$

where χ is an index for any of the three axes. This is a Gaussian distribution that is centered about each intrinsic angle and has standard deviation $\sigma_\chi = (k_B T/k_\chi)^{1/2}$. This distribution is the angle bias that defines the ABC model. From it, one can compute the same statistics for the ABC model as for the FJC model (table 2), which is shown in the appendix.

The ABC model has two main uses. It is a convenient waypoint between the FJC model and the WLC model, described next. Also, it is a version of the WLC model that is well-suited for computational investigations because it uses discrete segments (e.g. [35, 49, 55]).

3.3. Wormlike chain model

Real cytoskeletal filaments and real DNA bend reasonably smoothly rather than with the abrupt kinks of the previously described models. The Kratky and Porod WLC model (figure 1(D)) captures this smooth bending by treating a filament as an ideal flexible thin rod [56, 57]. It is the ABC model in the limit of an infinite number of infinitesimal length segments, separated by infinitesimal joint angles. In close analogy to equation (8), the WLC bending energy density is [49]

$$\varepsilon(s) = \frac{\kappa_\phi}{2} [\alpha_\phi(s) - \alpha_\phi^\circ]^2 + \frac{\kappa_\theta}{2} [\alpha_\theta(s) - \alpha_\theta^\circ]^2 + \frac{\kappa_\psi}{2} [\alpha_\psi(s) - \alpha_\psi^\circ]^2. \quad (10)$$

Conversions between the variables in equation (8) and those here are: segment numbers became contour lengths with $s = jb$, bending angles became curvatures with $\alpha_\chi = a_\chi/b$, intrinsic angles became intrinsic curvatures with $\alpha_\chi^\circ = a_\chi^\circ/b$, bending and twisting spring constants became *flexural* and *torsional rigidities* with $\kappa_\chi = k_\chi b$, and the bending energy became the bending energy density with $\varepsilon(s) = E_j/b$ [49].

If the intrinsic bending curvatures equal zero, the WLC *orientation autocorrelation function*, which expresses the correlation of the local orientation of the filament at one point with that at another point, decays exponentially [12]. It is

$$C(s) = \langle \cos \theta \rangle = e^{-|s|/P}, \quad (11)$$

where s is the contour length between the two points, θ is the angle difference between the filament tangents at the two points, and P is the persistence length. This equation shows that points on a filament that are much closer than the persistence length are likely to have similar orientations, whereas those that are much farther are likely to have different orientations. The persistence length is typically defined through this equation [12, 35–37]. However, complications arise when filaments have intrinsic curvatures or are investigated with two-dimensional images, which is discussed in section 3.5.

The persistence length is the central parameter of the WLC model. For example, the rms end-to-end length relates to the persistence length as [41, 42]

$$\langle \mathbf{R}^2 \rangle^{1/2} = \sqrt{2LP - 2P^2(1 - e^{-L/P})}. \quad (12)$$

This value approaches L for filaments that are much shorter than their persistence lengths, as one would expect for nearly straight filaments, and $(2LP)^{1/2}$ for filaments that are much longer than their persistence lengths. This latter limit agrees with the FJC result (equation (2)) if the FJC segment length equals $2P$. For this reason, $2P$ is called the statistical Kuhn length of the WLC, denoted b_{Kuhn} (e.g. the conformational statistics of long DNA filaments can be computed equally accurately using equation (12) with P equal to 50 nm, or using equation (2) with b equal to 100 nm). The WLC entropic elasticity depends on the persistence length according to [58]

$$F = \frac{3k_B T}{2PL} x \quad (13)$$

for small displacements (note the similarity to equation (4)) and is closely approximated by [48]

$$F = \frac{k_B T}{P} \left[\frac{1}{4} \left(1 - \frac{x}{L} \right)^{-2} - \frac{1}{4} + \frac{x}{L} \right] \quad (14)$$

for large displacements. An exact solution, for all displacements, can be computed numerically from equations presented in [59]. Figure 2 shows that these elasticities agree well with experimental force–extension data for DNA [48] (see also work by Marko and Siggia [36, 59], who investigated DNA elasticity in greater detail).

The WLC model applies equally well to short and stiff filaments, such as most cytoskeletal filaments, as to long and flexible ones. However, different questions often arise with the short and stiff filaments, such as how much they are deflected by applied transverse forces, or how much compressive force will cause buckling. These questions are typically answered using the theory of thin beams, which is described in [12, 39, 60]. For example, Gittes *et al* used an equation from beam theory to calculate that the critical buckling force for a 10 μm long microtubule that is free to pivot at its ends is about 2 pN [37]. Although superficially very different, beam theory is based on the same assumptions as the WLC (e.g. equation (10)), making them two versions of the same underlying model.

3.4. Filament conformation experiments

Cytoskeletal filament and DNA mechanics (table 1) have been measured by several methods. The most reliable generally involve investigations of individual filaments, as opposed to bulk measurements such as dynamic light scattering and sedimentation velocity tests [32]. In one class of approaches, researchers image individual filament conformations, typically using fluorescently labeled filaments, and quantify their thermal fluctuations [37, 61–63]. In another, researchers manipulate filaments directly using atomic force microscopy [64], microfabricated cantilevers [65], magnetic beads [66], or optical traps [67]. Predictions from the WLC model have generally agreed well with experimental results. This is true

for actin [65, 68], DNA at several levels of packing [35], and desmin intermediate filaments [64]. However, the WLC is a very simple model so deviations from its predictions are expected and, in fact, usually observed (e.g. [69]). For example, forces do not diverge toward infinity as the extension approaches the contour length but, instead, filaments break apart in ways that are characteristic of the underlying filament structure.

To address some of the elasticity data deviations, Odijk [70] added a linear elastic stretch modulus term to the WLC model so that it would account for the *enthalpic elasticity* of the underlying filament. This enabled better fits to experimental DNA [67] and actin [65] elasticity data, particularly for highly stretched filaments. Wiggins and coworkers extended the WLC model in a different way [71, 72]. The persistence length of DNA is about 50 nm, so one would normally expect it to be quite stiff on much shorter length scales. However, using atomic force microscopy, these authors showed that tight bends are not as energetically costly as expected, which is consistent with the tightly folded DNA conformations that are observed in viral packaging, histone binding, and transcription regulation. They replaced the harmonic bending energies of the WLC model ($\epsilon \sim \alpha_x^2$, equation (10)) with absolute value ($\epsilon \sim |\alpha_x|$) and other ‘softer’ energy functions, which enabled better fits to the DNA conformation data, particularly on short length scales.

3.5. Persistence lengths and rigidities

The conventional persistence length definition, given above as the correlation length for the orientation autocorrelation function [12, 35–37], does not apply universally because it relies on the autocorrelation function being an exponential. It *is* exponential for filaments that do not have intrinsic curvatures and that are modeled with the ABC or WLC models (appendix and equation (11)). However, it is not an exponential for the FJC or GC models, so their persistence lengths are undefined ($C(s)$ is a step function for the FJC model, and a Gaussian for the GC model). It is also non-exponential for the ABC and WLC models when intrinsic filament curvatures are non-zero. To address these latter cases, I propose that twice the correlation length of the *orientation cross-correlation function* is a better persistence length definition. Here, one considers a statistical ensemble of filaments that all start with the same orientation and quantifies the angular correlations between different filaments at the same contour lengths from their starting points. The persistence length is twice the correlation length because correlations are considered between two filaments, both of which bend randomly. The orientation cross-correlation function is exponential in the WLC model even if filaments have intrinsic curvatures, shown in the appendix. This definition is identical to the conventional one when filaments are not intrinsically curved.

A separate issue arises for filaments in two dimensions. Howard [12] defines the persistence length for filaments in two dimensions as half of that for filaments in three dimensions. Although there is some logic to this definition, as described below, his definition nevertheless disagrees with that of most other authors [35, 36] and of its use here.

For the WLC model, the persistence length relates to the filament flexural rigidities according to (appendix and [32])

$$P = \frac{2\kappa_\phi\kappa_\theta}{k_B T(\kappa_\phi + \kappa_\theta)}. \quad (15)$$

In the typical case of rotationally symmetric filaments, the two transverse flexural rigidities, κ_ϕ and κ_θ , equal each other; they are typically just called the flexural rigidity and denoted κ . In this case, equation (15) simplifies to $P = \kappa/(k_B T)$ [32, 35, 37]. For filaments in two dimensions, such as membrane-bound cytoskeletal filaments, a filament can only bend on a single axis, say to its left or right. Using the Tait–Bryan angles, this means that the filament only bends on the yaw axis; this implies that the pitch flexural rigidity is effectively infinite, so the (two-dimensional) persistence length equals $2\kappa_\phi/(k_B T)$, from equation (15). The factor of two in this result arises from the fact that the filament can only bend on one axis instead of the two axes for filaments in three dimensions. (In practice though, the WLC can be an inaccurate model in two dimensions because of the increasing importance of long-range interactions, as shown by Maier and Rädler using membrane-bound DNA [73].)

A subtly different case concerns filaments that are rotationally symmetric and that exist natively in three-dimensional space, such as actin, but that are imaged with two-dimensional images. In this case, the images only show half of the filament bending, so the two-dimensional persistence lengths measured from the images need to halved to determine the filament's true three-dimensional persistence length [32, 37]. This factor of two is reflected in Howard's persistence length definitions mentioned above [12]. However, I suggest that it should not be included in persistence length definitions because it arises from the data analysis rather than physical reality.

Filaments can twist as well as bend. Twisting is characterized in a similar manner as bending. In particular, the *torsional persistence length*, P_{tor} , is the length over which thermal twisting fluctuations become substantial. A natural definition is the characteristic length of the torsional autocorrelation function,

$$C_{\text{tor}}(s) = \langle \cos \psi \rangle = e^{-|s|/P_{\text{tor}}}, \quad (16)$$

which expresses the correlation of the total filament twist at one point with that at another point; ψ is the twist difference and s is the contour length between the points. Alternatively, for filaments with intrinsic twists, the torsional persistence length is better defined as twice the characteristic length of the torsional cross-correlation function, as shown in the appendix.

The torsional persistence length relates to the torsional rigidity, κ_ψ (often denoted C), as (see appendix and [74])

$$P_{\text{tor}} = \frac{2\kappa_\psi}{k_B T}. \quad (17)$$

As with the bending persistence length for a filament in two dimensions, the factor of 2 in the numerator arises from the single degree of freedom for torsion. *However, this factor of 2 is nearly universally ignored.* In particular, Langowski's excellent review of DNA and chromatin models omits it [35], as do [75–77]. Most often, the torsional persistence length is

simply defined as $\kappa_\psi/k_B T$ and no reference is made to the torsional autocorrelation function.

Flexural and torsional rigidities relate to a filament's cross-sectional shape and material properties. If a filament has an isotropic composition, much like a thin metal rod, the rigidities are [39]

$$\kappa_\phi = I_\phi E \quad (18)$$

$$\kappa_\theta = I_\theta E \quad (19)$$

$$\kappa_\psi = JG, \quad (20)$$

where I_ϕ is the area moment of inertia for yaw-direction bending, I_θ is the area moment of inertia for pitch-direction bending, E is the material's Young's modulus, J is the torsional constant for the filament's cross-section, and G is the material's shear modulus (see [38, 39, 49, 50, 60]). On the further assumption that the filament can be treated as a solid cylinder of radius r , the rigidities simplify to

$$\kappa = \kappa_\phi = \kappa_\theta = \frac{\pi r^4 E}{4} \quad (21)$$

$$\kappa_\psi = \frac{\pi r^4 G}{2}. \quad (22)$$

Finally, the relationship $G = E/[2(1 + \nu)]$, where ν is Poisson's ratio [39], yields the following relationships between the torsional and flexural rigidities, and the torsional and flexural persistence lengths:

$$\kappa_\psi = \frac{2\kappa}{1 + \nu} \quad (23)$$

$$P_{\text{tor}} = \frac{4P}{1 + \nu}. \quad (24)$$

Poisson's ratio is the relative expansion that an isotropic material exhibits on the x and y axes when it is compressed along the z -axis. Poisson's ratio values are almost always between 0 and 0.5 [39] and are about 0.3 for typical synthetic polymers. Equation (24) shows that if cytoskeletal or DNA filaments can be treated as being essentially cylindrical and of isotropic compositions, then their torsional persistence lengths should be about three times their bending persistence lengths. This is in fact the case for DNA and actin, as shown in table 1. On the other hand, Chelminiak *et al* found that microtubule torsional persistence lengths are about a tenth of their bending persistence lengths, from modeling results [78]. They found that this high twisting flexibility arises from the combination of the helical structure and the hollow design of microtubules.

4. Filament dynamics

Biological filaments exhibit a wide range of interesting assembly and disassembly dynamics. DNA replication is particularly elaborate. In brief, DNA helicase separates the DNA into its component strands, DNA polymerase assembles the new strands using base pair matching, and multiple DNA topoisomerases relieve twisting [11, 79]. The result is replication at up to about 300 nm s^{-1} and a remarkably low basepair mismatch rate of about 1 in 10^9 . Microtubules exhibit length fluctuations called dynamic instability in which their

plus ends switch between persistent growth periods and bouts of rapid depolymerization [80–82]. Growth rates are roughly 110 nm s^{-1} , depending on tubulin concentrations and applied forces, while shrinkage rates are about 330 nm s^{-1} [83–85]. Actin's dynamics are dominated by treadmilling, at about 300 nm s^{-1} , in which filaments continually polymerize at their barbed (plus) ends and depolymerize at their pointed (minus) ends [14, 86]. Actin also branches frequently, forms cross-links between filaments, and terminates elongation with end-capping, which together create dense filament networks [2, 87]. Intermediate filaments are more stable than microtubules or actin but are also routinely rearranged and cross-linked, especially during processes such as cell spreading, wound healing, and cell division [88–90]. These dynamics likely take place, at least in part, through protein exchange between the cytoplasm and filament. The bacterial homologs of these eukaryotic filament proteins are structurally similar, but have different dynamics [18, 19, 91]. For example, the tubulin homolog FtsZ likely assembles into the cell division Z-ring through filament bundling processes and then dissociates from the Z-ring during ring constriction [92]; these behaviors are quite different from microtubule dynamic instability. Together, these processes show that biological filaments are not only highly dynamic, but often transient as well.

A separate filament dynamics topic concerns the conformations of individual filaments, which is the focus of the rest of this section. Biological filaments are invariably immersed in dense environments, such as cytoplasm or nucleoplasm. These environments are highly viscous for objects with the diameters of biological filaments (i.e. Reynolds numbers are very low [93]). They are also highly crowded with macromolecules and other filaments [94]. As a result, cytoskeletal and DNA filaments do not obey Newtonian dynamics, in which accelerations are proportional to forces. Instead, they obey Brownian dynamics, in which velocities are proportional to forces. Inertia is insignificant in this regime, while viscous drag and thermal forces are dominant.

4.1. Rouse and Zimm models

The *Rouse and Zimm models* [95, 96] are ‘spring-and-bead’ models that treat the environment as an ideal viscous fluid. They represent a filament's conformation using a GC, which forms the models' springs, and they represent the filament's volume using beads at the segment joints (figure 4). Three forces act on each bead [41, 42]. (i) Each spring exerts a tension force on its connected beads with force constant $3k_B T/b^2$ (equation (7)). (ii) The fluid exerts random thermal forces, \mathbf{f} , that act on the beads from the Brownian motion of the fluid molecules; these forces are Gaussian distributed and are uncorrelated both between beads and over time. (iii) The fluid exerts drag forces on the beads that are proportional to, and opposite, the beads' velocity. Here, the models differ. The Rouse model, called the free-draining case, ignores all hydrodynamic interactions between beads so that the drag force on each bead equals ζ , the bead drag coefficient, times the negative of the bead's velocity. Stokes's Law gives this

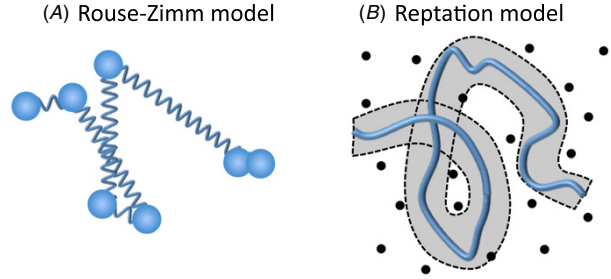


Figure 4. Filament dynamics models. (A) The Rouse and Zimm models represent filaments with ‘spring-and-bead’ models, which extend the Gaussian chain model. Wiggly lines represent springs and balls represent beads. (B) The reptation model addresses filament confinement by external immobile constraints, shown with black dots, which might represent other filaments or macromolecules in a crowded cytoplasm. These constrain the filament to move solely within the shaded tube that is outlined with a dashed line.

drag coefficient as $\zeta = 6\pi\eta r$, where η is the solvent viscosity and r is the bead radius. The Zimm model, which is also called the Rouse–Zimm model and is the non-draining case, takes the opposite approach of assuming strong hydrodynamic interactions between the beads (see [41] or [42] for details). Using theoretical arguments, De Gennes predicted that the Rouse model should be more accurate for extended filaments while the Zimm model should be more accurate for collapsed filaments [97].

Focusing on the simpler Rouse model for now, the three forces combine to yield the following *Langevin equation of motion* [41],

$$\zeta \dot{\mathbf{r}}_j = -\frac{3k_B T}{b^2} (2\mathbf{r}_j - \mathbf{r}_{j-1} - \mathbf{r}_{j+1}) + \mathbf{f}_j \quad (25)$$

where \mathbf{r}_j is the position of the j th bead. This equation applies to internal beads; the factor in parentheses is replaced by $(\mathbf{r}_1 - \mathbf{r}_2)$ for the first bead and by $(\mathbf{r}_n - \mathbf{r}_{n-1})$ for the last bead. The three terms in this equation of motion, including the term on the left side of the equals sign, reflect the drag, elastic, and thermal forces, respectively. This equation cannot be simplified to give the motion of each bead independently because each bead is coupled to its neighbors. Instead, Rouse solved it by finding the system's normal modes, of which the zeroth mode represents diffusion of the entire filament, D , and the first mode represents the slowest relaxation time of the filament, τ [95].

Sparing the mathematical details, the Rouse model diffusion coefficient and slowest relaxation times are [41]

$$D_R = \frac{k_B T}{6\pi\eta r N} \sim L^{-1} \quad (26)$$

$$\tau_R = \frac{2\eta r N^2 b^2}{\pi k_B T} \sim L^2. \quad (27)$$

The first equation follows from the Einstein relation, which states that the diffusion coefficient equals $k_B T$ divided by the drag coefficient, and the drag for N beads that do not have hydrodynamic interactions with each other is N times the drag for one bead. As a result, the diffusion coefficient scales inversely with the filament's contour length. The relaxation time reflects the time for the filament to diffuse over a distance

that is proportional to the total filament ‘radius’, such as the rms end-to-end length. This means that $\tau \sim \langle \mathbf{R}^2 \rangle / D \sim Nb^2 / D \sim \eta r N^2 b^2 / k_B T$, where the second proportionality follows from equation (2) and the third from equation (26); the result is clearly similar to equation (27). The relaxation time scales with the square of the filament’s contour length. The bead radius in these equations does not relate well to molecular parameters [98], but can be estimated by making the total bead volume equal the total filament volume [99, 100].

The corresponding Zimm model solutions [41] are

$$D_Z = \frac{8k_B T}{3(6\pi^3)^{1/2} \eta b \sqrt{N}} \sim L^{-1/2} \quad (28)$$

$$\tau_Z \sim \frac{N^{3/2} b^3 \eta}{k_B T \sqrt{3\pi}} \sim L^{3/2}. \quad (29)$$

This diffusion coefficient also has a relatively simple interpretation. Recalling that the linear extent of a long random filament grows as the square root of the total contour length (equation (2)), this shows that the Zimm model diffusion coefficient is inversely proportional to the filament coil’s radius. Also, the Stokes–Einstein equation ($D = k_B T / (6\pi \eta r)$) states that the diffusion coefficient of a sphere is inversely proportional to the sphere’s radius. Putting these together, the Zimm model predicts that a filament should diffuse like a solid sphere which has a radius equal to $3\pi^{1/2}/8 \approx 0.66$ times the filament’s radius of gyration. In other words, filament diffusion in dilute solutions can be envisioned as the diffusion of a monolithic filament cluster, albeit one with internal motions. The relaxation time is more difficult to interpret. However, it is worth noting that the two Zimm model results scale more slowly with filament length than the two Rouse model results. This reflects the fact that hydrodynamic interactions between the beads create locally correlated fluid motions, which decreases the drag on each bead.

4.2. Stiff rod and dynamic wormlike chain models

The spring-and-bead foundations of the Rouse and Zimm models are convenient but inaccurate representations of reality, applying only when filaments are extremely long. Focusing on the opposite extreme for now, on filaments that are significantly shorter than their persistence lengths, a better representation is a reasonably stiff cylindrical rod. Rods have many fewer degrees of freedom than flexible filaments, so they are easier to treat theoretically. Stiff rods have three separate diffusion coefficients, which are for rotation, translation parallel to the rod’s long axis, and translation perpendicular to the rod’s long axis. These can be combined to give the overall translational diffusion coefficient, which is [41, 101–103]

$$D_{\text{rod}} = \frac{k_B T [\ln(L/2r) + \nu]}{3\pi \eta L} \sim \frac{\ln L + \text{constant}}{L}, \quad (30)$$

where L and r are the rod length and radius, respectively. The ν parameter, which is small and often ignored [41], addresses the hydrodynamics at the rod ends and is a function that depends weakly on $L/2r$ (numerical results suggest that it can be closely approximated by $0.312 + 0.565/p - 0.050/p^2$, where p equals $L/2r$ [103]). The dependence of this diffusion coefficient

on the filament length is intermediate between those of the Rouse and Zimm models. This makes sense because it treats hydrodynamic interactions accurately, rather than assuming the weak or strong limits.

The relaxation time constants for a reasonably stiff rod have also been computed, in this case from the hydrodynamic beam equation, which comes from the theory of thin beams [12]. For a free filament, meaning one that is not clamped at either end, the slowest relaxation time constant is

$$\tau_{\text{rod}} \approx \frac{4\pi \eta}{P k_B T [\ln(L/2r) + 0.84]} \left[\frac{L}{4.73} \right]^4 \sim \frac{L^4}{\ln L + \text{constant}}. \quad (31)$$

This equation combines the time constant equation, which is $\tau_{\text{rod}} = (\gamma/\kappa)(L/q_n)^4$, with the drag coefficient per unit length, which is $\gamma = 4\pi \eta / [\ln(L/2r) + 0.84]$, the q_n factor, which is about 4.73 for the slowest relaxation time of an unclamped filament, and the persistence length for a rotationally symmetric filament, which is given above near equation (15) (see [12, 104, 105]). This relaxation time has a much stronger length dependence than either the Rouse or Zimm models. This difference reflects the fact that the restoring force derives from the rod bending energy here whereas it arose from entropic factors during chain extension for the Rouse and Zimm models [98].

The stiff rod model has been shown to agree reasonably well with microtubule and actin shape fluctuations [104, 105]. For example, Janson and Dogterom [104] analyzed microtubule images using the stiff beam relaxation times to determine microtubule persistence lengths; they found that fast-growing microtubules are less stiff than slow-growing ones. They also found some deviations from the stiff rod model, which they suggested might arise from friction within microtubules.

A more general approach to addressing the failings of the Rouse and Zimm models has been to compute the dynamics of the WLC model. In concept, this generalizes the stiff rod model from very short filaments to filaments that are as long as or longer than their persistence lengths. Pioneering work on *dynamic* WLC models by Harris and Hearst [106] has been improved upon by several researchers, leading to models that both ignore [107–109] and include hydrodynamic interactions [98, 110]. Of these, a model by Harnau *et al* [98] appears to be particularly successful because it does not have internal inconsistencies that others have and it agrees well with experimental data, as described below. As section 3.3 mentions, the *conformational* statistics of the WLC vary continuously between those of a stiff rod for short filaments to those of the FJC for long filaments; similarly, the *dynamical* predictions of Harnau *et al*’s dynamic WLC model vary continuously between those of a stiff rod for short filaments (equations (30) and (31)) to those of the Zimm model (equations (28) and (29)) for long filaments. It also enables predictions for filaments that are in between these limits. Unfortunately though, Harnau *et al*’s dynamic WLC model has the drawback that it is inconvenient to use because the diffusion coefficient and relaxation times (equations (3.13) and (4.12), respectively, in [98]) have only been given as integral

equations that require numerical evaluation. Approximating these equations with closed-form solutions is an obvious direction for future research.

4.3. Filament dynamics experiments

Filament dynamics have been investigated extensively with experiments. Those that have studied DNA have been particularly informative because DNA can be synthesized or isolated with essentially any desired length with, importantly, a very narrow length distribution [111]. For short filaments (down to eight basepairs), diffusion coefficients are generally measured using dynamic light scattering [112] or fluorescence correlation spectroscopy [113, 114], while long filaments (up to 309 000 basepairs) are best investigated with single molecule techniques [47]. In brief, experiments almost always show that diffusion coefficients decrease with increasing filament length according to a power law that has a slope between -0.6 and -0.7 [47, 115, 116]. These do not agree with either the Rouse or Zimm models. However, these data do fit well to Harnau *et al.*'s dynamic WLC model [116]. Diffusion data also agree well with the stiff rod limit for short filaments [112] and they approach the Zimm model limit for long filaments [47].

Experiments on DNA relaxation [116–118] show the same qualitative results, agreeing well with Harnau *et al.*'s dynamic WLC model over the entire length range. In a particularly interesting example, long filaments that started out highly extended relaxed according to Zimm type dynamics [117]; this contrasted De Gennes's prediction [97] that they would obey Rouse type dynamics.

These results, together with those mentioned above, tell a consistent story. DNA, actin, microtubules, and presumably most other filaments show strong within-filament hydrodynamic interactions when in dilute solutions. Their dynamics agree well with the stiff rod model if they are very short ($L < P/10$), with the Zimm model if they are very long ($L > 100P$), and with Harnau *et al.*'s dynamic WLC model for all lengths. These results are also consistent with recent modeling results on protein diffusion. Strong hydrodynamic effects are observed both in dilute solutions [119] and in crowded cytoplasm [120].

4.4. Reptation

The successes of the dynamic WLC models are tempered by the observation that DNA in cytoplasm and nucleoplasm does not diffuse as it does in dilute solution [115]. Instead, experiments show that motility decreases very rapidly with increasing filament length, likely from entanglement or sieving effects. The *reptation model* addresses these effects. It assumes that a filament is effectively confined to a tube that is bounded by a field of obstacles [121]. The filament can distort freely within the tube, and it can diffuse along the tube's contour, but it cannot escape the tube by moving laterally. By considering the difference between the tube length and the filament contour length, De Gennes realized that the excess 'slack' filament length would form wiggles in the tube that would diffuse back and forth along the filament (much like the arch of

a caterpillar moves along a caterpillar [41]). Based on this motion, De Gennes found that the filament diffusion coefficient and relaxation times in the reptation model are [41]

$$D_{\text{rept.}} = \frac{k_B T a^2}{3N^2 \zeta b^2} \sim L^{-2} \quad (32)$$

$$\tau_{\text{rept.}} = \frac{\zeta N^3 b^4}{\pi^2 k_B T a^2} \sim L^3. \quad (33)$$

Here, a is the effective segment length of the tube; it is analogous to the Kuhn length of the filament, b_{Kuhn} , but is for the tube rather than for the filament. It is on the order of the mean distance between obstructions [41]. The strong dependences of the diffusion coefficient and relaxation times on the filament length, relative to those of the Rouse and Zimm models shown above, shows that obstacles strongly limit the motility of long filaments.

Reptation has been experimentally observed for DNA [122] and actin [68, 123]. In the DNA experiments, Perkins and coworkers [122] used optical tweezers to drag one end of a fluorescently labeled DNA filament through an entangled solution of other DNA filaments. They observed that the labeled filaments became stretched out, got dragged along, and then collapsed again, all while staying close to the original filament contour. These results suggested that filament confinement was consistent with the reptation tube model. Similarly, Käs and coworkers [68, 123] imaged individual fluorescently labeled actin filaments in entangled solutions of unlabeled actins. Their images of filament displacements over time were also consistent with the reptation tube model.

4.5. Computational filament dynamics

The level of detail represented by filament models is severely limited by mathematical tractability. In particular, it is difficult to combine the analytical models described above with external filament influences, such as those that arise from pores, membranes, and molecular motors. Computational modeling often presents the best solutions to these problems. Algorithms that simulate filament conformational dynamics are essential to many such studies, and are the focus of this section.

Computational models typically represent filaments using a version of the ABC model (e.g. [35, 49, 55, 124]). They include bending forces at filament joints (equation (8)) and sometimes also stretching forces within segments. Models typically represent the filament's hydrodynamic drag either by treating each segment as a cylinder as in the stiff rod model (e.g. [124, 125]) or by using beads at the segment joints as in the Rouse and Zimm models (e.g. [35, 50, 51, 74, 126, 127]). The former case is more accurate whereas the latter is simpler.

Dynamics simulations are almost invariably based upon a Langevin type equation of motion, as in equation (25), in which segment or bead velocities are proportional to the forces that are incident upon them. These forces always include thermal and drag effects from the fluid that surrounds the filament. They may also include one or more of the following [35, 50, 51, 55]: joint bending and twisting torques, segment stretching forces, chemical or electrostatic interaction forces between different filament portions, and interaction forces between the

filament and membranes or other filaments. Hydrodynamic interactions, if included in the model at all, are usually based on hydrodynamic interaction tensors [35, 50, 51].

Integrating the Langevin equation to yield segment positions from segment velocities is simple in principle but challenging in practice due to coupling between the segments. Furthermore, most filaments respond to stretching on a much faster timescale than to filament bending (a direct consequence of the theory of thin beams, which shows that stretching distortions typically propagate at up to about L/r times faster than bending distortions [39]). This wide difference in timescales leads to so-called stiff differential equations, which are notoriously difficult to integrate. The two basic classes of solution methods are *explicit and implicit methods* [128].

In explicit methods, the filament position at the next time point is computed from its velocity at the current time point. The classic and simple forward Euler method is an explicit method [55], as are the higher order Runge–Kutta and velocity Verlet methods [50, 129] (in this context, these methods are sometimes called second order Brownian dynamics). The latter ones work with velocities at multiple times, rather than just at the current simulation time, to enable better predictions and hence longer simulation time steps. All of these explicit methods have the advantage of treating segments independently, which enables them to work easily with ‘complex’ filaments, including branched and cross-linked filament networks, elastic filaments, and filaments with constrained motion. On the other hand, the stiffness of the underlying differential equations necessitates the use of time steps that are shorter than the fastest filament dynamics timescales to avoid numerical instabilities, often leading to steps on the order of nanoseconds [50, 129]. To reduce the high computational demands of such short time steps, Hörger and coworkers [55] used unphysically elastic filaments. This reduced differential equation stiffness, which enabled microsecond length time steps. Analogously, Kierfeld and coworkers used unphysically viscous solutions [125], which again reduced differential equation stiffness and enabled longer time steps.

Implicit integration methods address the coupling between segments by treating all segments simultaneously in a multidimensional linear equation [128]. Solving this equation by matrix inversion is very computationally expensive, so it is typically solved with the biconjugate gradient stabilized method instead [130, 131]. It is possible to include all of the same forces and interactions when using implicit integration methods as explicit ones, but the biconjugate gradient solution methods are much faster when the linear equation matrix is sparse. Thus, it is advantageous to assume that all segments are the same length, that they are inelastic, that there are no long-range interactions, and that filaments are minimally branched or cross-linked. Doing so enables excellent numerical stability and accurate simulation with very long time steps, often on the order of tens of ms [131].

A final integration method is the *PAIRS method* [132]. It is an explicit method, based on the forward Euler method, which makes it simple and versatile. However, in contrast to the other explicit methods, the PAIRS method does not base its

computations on the actual segment forces, but on the forces multiplied by so-called PAIRS coefficients. These coefficients are calibrated to account for the forward Euler method errors. Using them, simulation results are exact for filaments with two segments and reasonably accurate for longer filaments. As a result, simulations can use time steps of 0.1 ms [133] without substantial errors or numerical instabilities. Although the PAIRS method is an attractive alternative to the standard implicit and explicit methods, it has only been used in a few studies [133, 134] and it has not received a strong theoretical investigation, so its capabilities remain largely unknown.

5. Summary and outlook

Despite its foundation in polymer theory, which has been investigated for most of a century, much still remains to be discovered in the science of biological filaments. It is clear at this point that the WLC model is a reasonably good filament configuration model for a wide range of biological filaments, including DNA and most cytoskeletal filaments. It is also clear that hydrodynamic interactions within filaments are quite strong when the filaments are in dilute solutions, and that reptation dynamics arise when filament motion is tightly constrained. However, all of the key experiments that showed these results were performed with *in vitro* systems, leaving quantitative filament dynamics in native cellular environments still largely unexplored. Unlike *in vitro* systems, cells are highly crowded with macromolecules, which affects intracellular diffusion coefficients, chemical reaction rates, protein folding rates, and, almost certainly, filament dynamics [94, 135]. Also, cells are not the infinite volumes that polymer theorists often prefer, but are small confined volumes, replete with internal membranes. Finally, cytoskeletal filaments rarely function as individuals, but are typically components of dense filamentous structures, such as actin gels or mitotic spindles.

Likewise, much remains to be done in developing filament computational methods. Here, the basic algorithmic designs have likely been developed by now. In brief, a computer represents filaments using discrete chains of segments and it simulates filament dynamics by: computing the total forces on each segment, computing segment velocities from these forces, and integrating velocities over time to compute filament motion. However, current integration methods are largely inadequate for simulating large numbers of cellular filaments over biologically relevant timescales. Explicit methods are computationally intensive while implicit methods do not handle realistic filament complexity very well. Thus, the modeling community needs new integration methods that enable both speed and versatility. These modeling methods need to be integrated into software that simulates other cell processes as well so that researchers can investigate the interactions between filaments and the cellular environment.

The centrality of filaments to cell biology, combined with the many open questions in the field, suggest that this will be an active research area for many years to come.

Acknowledgments

Thanks are due to many colleagues for helpful discussions, including particularly: Jane Lipson, John Finn, Jonathan Alberts, Adam Arkin, Alex Mendenhall, Bill Peria, and Roger Brent. This work was funded in part by National Institute of General Medical Science grant R01 GM0866615, awarded to Roger Brent and Richard Yu.

Appendix

This appendix presents new derivations for several conformational statistical results of the ABC model.

To enable simple mathematical filament representation, the Tait–Bryan angles for each joint, from equation (8), are combined to yield the direction cosine matrix [54],

$$\mathbf{A}_j = \begin{bmatrix} c a_\theta c a_\phi & c a_\theta s a_\phi & -s a_\theta \\ s a_\psi s a_\theta c a_\phi - c a_\psi s a_\phi & s a_\psi s a_\theta s a_\phi + c a_\psi c a_\phi & c a_\theta s a_\psi \\ c a_\psi s a_\theta c a_\phi + s a_\psi s a_\phi & c a_\psi s a_\theta s a_\phi - s a_\psi c a_\phi & c a_\theta c a_\psi \end{bmatrix}, \quad (\text{A.1})$$

where c represents cosine and s represents sine. The j subscripts were omitted from the a_χ variables here for brevity, but each of these angles still represent rotations at a single filament joint. Assume that the first segment's long axis has orientation \mathbf{e}_1 , where \mathbf{e}_1 is the unit column vector (1,0,0). Segment number 2 is rotated from \mathbf{e}_1 by angles $a_{\theta,2}$, $a_{\phi,2}$ and $a_{\psi,2}$, meaning that it is parallel to $\mathbf{A}_2 \mathbf{e}_1$. By extension, the n th segment is parallel to $\mathbf{A}_n \mathbf{A}_{n-1} \dots \mathbf{A}_2 \mathbf{e}_1$.

The orientation autocorrelation function is the product of the initial segment orientation vector with that of the n th segment, averaged over all possible filament conformations [136]. It is

$$C_n = \langle \mathbf{e}_1^T \mathbf{A}_n \mathbf{A}_{n-1} \dots \mathbf{A}_2 \mathbf{e}_1 \rangle. \quad (\text{A.2})$$

The average accounts for all $a_{\chi,j}$ values at all joints. These are independent and identically distributed random variables, enabling the simplification

$$C_n = \mathbf{e}_1^T \langle \mathbf{A} \rangle^{n-1} \mathbf{e}_1. \quad (\text{A.3})$$

The average direction cosine matrix, $\langle \mathbf{A} \rangle$, is computed by averaging the $\cos(a_\chi)$ and $\sin(a_\chi)$ values using the Gaussian-distributed weighting given in equation (9),

$$\langle \cos a_\chi \rangle = \int_{-\infty}^{\infty} \frac{1}{\sigma_\chi \sqrt{2\pi}} e^{-\frac{(a_\chi - a_\chi^o)^2}{2\sigma_\chi^2}} \cos a_\chi da_\chi = e^{-\frac{\sigma_\chi^2}{2}} \cos a_\chi^o \quad (\text{A.4})$$

$$\langle \sin a_\chi \rangle = \int_{-\infty}^{\infty} \frac{1}{\sigma_\chi \sqrt{2\pi}} e^{-\frac{(a_\chi - a_\chi^o)^2}{2\sigma_\chi^2}} \sin a_\chi da_\chi = e^{-\frac{\sigma_\chi^2}{2}} \sin a_\chi^o. \quad (\text{A.5})$$

Combining these results with equation (A.1) leads to a lengthy solution for $\langle \mathbf{A} \rangle$. Thus, we assume that the intrinsic joint angles, a_θ^o , a_ϕ^o and a_ψ^o equal zero, which simplifies $\langle \mathbf{A} \rangle$ to

$$\langle \mathbf{A} \rangle = \begin{bmatrix} e^{-(\sigma_\theta^2 + \sigma_\phi^2)/2} & 0 & 0 \\ 0 & e^{-(\sigma_\psi^2 + \sigma_\phi^2)/2} & 0 \\ 0 & 0 & e^{-(\sigma_\theta^2 + \sigma_\psi^2)/2} \end{bmatrix}. \quad (\text{A.6})$$

Finally, combining this with equation (A.3) yields the orientation autocorrelation function,

$$C_n = e^{-(n-1)(\sigma_\theta^2 + \sigma_\phi^2)/2} = e^{-(s-b)(\sigma_\theta^2 + \sigma_\phi^2)/2b} \quad (\text{A.7})$$

where the contour length, s , equals nb . The latter form is better written as $C(s)$, but has the caveat that it is only strictly correct if s is an integral multiple of b . The orientation autocorrelation function exhibits simple exponential decay with correlation length equal to $2b/(\sigma_\theta^2 + \sigma_\phi^2)$.

Computing the orientation *cross*-correlation function, as suggested in section 3.5, is very similar. Consider a second filament that also starts with orientation \mathbf{e}_1 . Using \mathbf{A}'_j for its direction cosine matrices, its n th segment is parallel to $\mathbf{A}'_n \mathbf{A}'_{n-1} \dots \mathbf{A}'_2 \mathbf{e}_1$. The product of the two n th segment vectors, averaged over all possible filament conformations, is the cross-correlation function,

$$X_n = \langle \mathbf{e}_1^T \mathbf{A}'_2{}^T \dots \mathbf{A}'_{n-1}{}^T \mathbf{A}'_n{}^T \mathbf{A}_n \mathbf{A}_{n-1} \dots \mathbf{A}_2 \mathbf{e}_1 \rangle. \quad (\text{A.8})$$

This simplifies to

$$X_n = \mathbf{e}_1^T (\langle \mathbf{A} \rangle^T \langle \mathbf{A} \rangle)^{n-1} \mathbf{e}_1. \quad (\text{A.9})$$

The matrix product, again invoking the assumption that the intrinsinc angles equal zero, is found from equation (A.6) to be

$$\langle \mathbf{A} \rangle^T \langle \mathbf{A} \rangle = \begin{bmatrix} e^{-(\sigma_\theta^2 + \sigma_\phi^2)} & 0 & 0 \\ 0 & e^{-(\sigma_\psi^2 + \sigma_\phi^2)} & 0 \\ 0 & 0 & e^{-(\sigma_\theta^2 + \sigma_\psi^2)} \end{bmatrix}. \quad (\text{A.10})$$

Combining with equation (A.9) yields the orientation cross-correlation function,

$$X_n = e^{-(n-1)(\sigma_\theta^2 + \sigma_\phi^2)} = e^{-(s-b)(\sigma_\theta^2 + \sigma_\phi^2)/b}. \quad (\text{A.11})$$

This is identical to the autocorrelation function in equation (A.7), except that the correlation length is half as long. This difference arises from the fact that two filaments are considered here, both of which include random bending, whereas only one filament was considered in the autocorrelation function.

The persistence length is the correlation length of the orientation autocorrelation function, or twice the correlation length of the orientation cross-correlation function, both of which give

$$P = \frac{2b}{\sigma_\theta^2 + \sigma_\phi^2} = \frac{2bk_\theta k_\phi}{k_B T (k_\theta + k_\phi)}. \quad (\text{A.12})$$

Similar analyses yield the torsional auto- and cross-correlation functions. The only changes are: (i) the overlap of vectors that are perpendicular to the segment long axes are considered rather than of those that are parallel to the segment long axes and (ii) only effects that arise from filament torsion are included. These are accomplished by bracketing the matrix products in equations (A.2) and (A.8) with the \mathbf{e}_2 vectors, where \mathbf{e}_2 is defined as the (0,1,0) column vector, and also only considering ψ rotations. Doing so leads to the ψ portion of the second diagonal element of equations (A.6) or (A.10), which yields

$$C_{\text{tor},n} = e^{-(n-1)\sigma_\psi^2/2} = e^{-(s-b)\sigma_\psi^2/2b} \quad (\text{A.13})$$

$$X_{\text{tor},n} = e^{-(n-1)\sigma_\psi^2} = e^{-(s-b)\sigma_\psi^2/b}. \quad (\text{A.14})$$

The correlation lengths are $2b/\sigma_\psi^2$ and b/σ_ψ^2 , respectively. As above, the persistence length is the former value, or twice the latter value, which is

$$P_{\text{tor.}} = \frac{2b}{\sigma_\psi^2} = \frac{2bk_\psi}{k_B T}. \quad (\text{A.15})$$

In order to compute the filament's mean squared end-to-end vector, it is convenient to change the filament definition slightly. Assume that the first segment is not parallel to \mathbf{e}_1 , but is rotated away from it by the direction cosine matrix \mathbf{A}_1 ; this clearly has no effect on the end-to-end length. With this change, the end-to-end vector is the sum of the vectors that represent the individual segments, which is

$$\mathbf{R} = \sum_{j=1}^n b\mathbf{A}_j\mathbf{A}_{j-1} \cdots \mathbf{A}_1\mathbf{e}_1. \quad (\text{A.16})$$

Squaring, averaging, and simplifying gives the mean squared end-to-end vector:

$$\begin{aligned} \langle \mathbf{R}^2 \rangle &= \left\langle \left(\sum_{k=1}^n b\mathbf{e}_1^T \mathbf{A}_1^T \cdots \mathbf{A}_{k-1}^T \mathbf{A}_k^T \right) \left(\sum_{j=1}^n b\mathbf{A}_j \mathbf{A}_{j-1} \cdots \mathbf{A}_1 \mathbf{e}_1 \right) \right\rangle \\ &= b^2 \sum_{j=1}^n \sum_{k=1}^n \mathbf{e}_1^T \langle \mathbf{A}_1^T \cdots \mathbf{A}_{k-1}^T \mathbf{A}_k^T \mathbf{A}_j \mathbf{A}_{j-1} \cdots \mathbf{A}_1 \rangle \mathbf{e}_1 \\ &= b^2 n + 2b^2 \mathbf{e}_1^T [(n-1)\langle \mathbf{A} \rangle + (n-2)\langle \mathbf{A} \rangle^2 + \cdots \\ &\quad + \langle \mathbf{A} \rangle^{n-1}] \mathbf{e}_1 \\ &= b^2 n + 2b^2 \mathbf{e}_1^T [\langle \mathbf{A} \rangle (\langle \mathbf{A} \rangle^n - n\langle \mathbf{A} \rangle \\ &\quad + n\mathbf{1} - \mathbf{1})(\mathbf{1} - \langle \mathbf{A} \rangle)^{-2}] \mathbf{e}_1 \end{aligned} \quad (\text{A.17})$$

where $\mathbf{1}$ is the identity matrix. The middle step uses the orthogonality of the direction cosine matrix to simplify $\mathbf{A}_j^T \mathbf{A}_j = \mathbf{1}$. Assuming no intrinsic joint angles, substituting in equation (A.6) and simplifying gives the result

$$\langle \mathbf{R}^2 \rangle = \frac{Lb \sinh \frac{b}{p} - b^2(1 - e^{-L/p})}{\cosh \frac{b}{p} - 1}. \quad (\text{A.18})$$

In the case of a long filament, the exponential term decays away to zero. Comparing the result to the FJC mean-square end-to-end distance, which is Lb from equation (2), shows that the statistical Kuhn length for the ABC model is

$$b_{\text{Kuhn}} = b \coth \frac{b}{2p}. \quad (\text{A.19})$$

Considering all of these results together, two limiting cases are particularly informative. First, if the angle bias is removed, meaning that each of the σ_χ values is increased toward infinity (or, equivalently, all of the k_χ values are decreased toward zero), these results approach those of the FJC. In particular, $\langle \mathbf{R}^2 \rangle$ approaches Lb , b_{Kuhn} approaches b , and the correlation functions approach 1 for unit n and 0 for larger n . The persistence lengths, which are undefined for the FJC, approach 0.

Secondly, if the segment lengths are made very short, meaning that b is reduced toward zero, all of these results approach those of the WLC. Those results are given in sections 3.3 and 3.5 and in table 2. Importantly, several of the statistics are more general in the WLC limit than they are for the ABC model because they also apply in the cases of non-zero intrinsic curvatures. To first order in b , equations (A.4) and (A.5) equal

$$\langle \cos a_\chi \rangle = e^{-\frac{\sigma_\chi^2}{2}} = 1 - \frac{bk_B T}{2k_\chi} \quad (\text{A.20})$$

$$\langle \sin a_\chi \rangle = \alpha_\chi^\circ b. \quad (\text{A.21})$$

Combining these solutions with the direction cosine matrix in equation (A.1), $\langle \mathbf{A} \rangle$ equals

$$\langle \mathbf{A} \rangle = \begin{bmatrix} e^{-\frac{\sigma_\phi^2 + \sigma_\psi^2}{2}} & \alpha_\phi^\circ b & -\alpha_\theta^\circ b \\ -\alpha_\phi^\circ b & e^{-\frac{\sigma_\phi^2 + \sigma_\psi^2}{2}} & \alpha_\psi^\circ b \\ \alpha_\theta^\circ b & -\alpha_\psi^\circ b & e^{-\frac{\sigma_\phi^2 + \sigma_\psi^2}{2}} \end{bmatrix} \quad (\text{A.22})$$

to first order in b . Using this, $\langle \mathbf{A} \rangle^T \langle \mathbf{A} \rangle$ equals equation (A.10), again to first order in b . However, no assumptions are now made about the intrinsic curvatures. Because this is the same equation as before, it leads to the same cross-correlation functions and persistence lengths that are shown in equations (A.11), (A.12), (A.14) and (A.15). Taking the limit of b going to zero, the persistence lengths approach equations (15) and (17) from the main text, but are now valid even with non-zero intrinsic curvatures.

Glossary

Actin filaments. Thin eukaryotic filaments composed of actin protein. Cytoskeletal versions are called microfilaments and muscle versions are called thin filaments.

Angle-biased chain. Filament conformation model that assumes discrete rigid segments and flexible joints that are biased toward specific angles.

Contour length. Total length of a filament, when measured along the filament's contour.

Enthalpic elasticity. Restoring force exhibited by a filament that arises from bending or stretching energy increases that occur when the filament is stretched.

Entropic elasticity. Restoring force exhibited by a filament that arises from the decrease in configurational entropy that occurs when the filament is stretched.

Euler angles. Three angles that describe the orientation of a rigid body. Rotations are about the z -axis, the old x -axis, and then the new z -axis, sequentially (using the x -convention).

Explicit integration. Numerical integration methods in which the state of a system at a future time point is computed from the state at the current time point.

Flexural rigidity. The sideward force required to bend a filament to unit curvature.

Freely jointed chain. Filament conformation model that assumes discrete rigid segments and unconstrained joints. Also called random flight model.

Gaussian chain. Filament conformation model that assumes discrete elastic segments and unconstrained joints, and that forms the basis of the spring-and-bead model.

Implicit integration. Numerical integration methods in which the state of a system at a future time point is found by solving an equation that relates the current and future states.

Intermediate filaments. A diverse class of flexible eukaryotic cytoskeletal filaments. Named for the fact that their diameters are intermediate between those of actin and microtubules.

Intrinsic angles and intrinsic curvature. The former are rotation angles for joints in the angle-biased chain model that minimize the respective energies, and the latter are analogous

curvatures in the wormlike chain model. Also called preferred angles and curvatures.

Kuhn length. Segment length in the freely jointed chain model that yields the same rms end-to-end length as that found in some other model, usually taken in the limit of long filaments.

Langevin equation. Equation of motion that includes a sum of deterministic and stochastic forces (which exhibit a Gaussian probability distribution and a Dirac delta function time correlation function), of which the latter typically arise from Brownian motion.

Long-range interactions. Interactions between filament regions that are widely separated along the filament's contour, including regions that are physically proximate due to filament bending.

Microtubules. Hollow and stiff eukaryotic cytoskeletal filaments composed of tubulin protein.

Orientation autocorrelation function. Function that expresses the correlation of the local orientation of a filament at one point with that at another point.

Orientation cross-correlation function. Function that expresses the correlation of the local orientation of a filament at some contour length with that of another filament at the same contour length.

PAIRS integration. Explicit numerical integration method in which differential equation parameters are replaced by so-called PAIRS coefficients, which are calibrated to minimize numerical errors.

Persistence length. Filament stiffness, measured as the length along the filament's contour where thermal bending or twisting influences become substantial. Typically defined as the statistical correlation length for the relative filament orientations at two points along the filament's contour. Bending degrees of freedom are typically assumed unless torsion is specified.

Radius of gyration. Root mean square filament radius, taken relative to the filament's center of mass, while considering all portions of the filament. Typically refers to the mean value of a statistical ensemble of filament conformations.

Reptation model. Filament dynamics model that accounts for restricted filament motion by treating the filament as though it is inside a tube.

Root mean squared (rms) end-to-end distance. Average straight-line distance between the two ends of a filament, computed using a statistical ensemble of conformations and the root mean square averaging method.

Rouse model. Filament dynamics model that treats filaments with 'springs and beads', and that neglects hydrodynamic interactions between the beads (called the free-draining assumption).

Short-range interactions. Interactions between filament regions that are closely spaced along a filament's contour.

Tait-Bryan angles. Three angles that describe the orientation of a rigid body, often used for ships and airplanes. Rotations are about the z -axis, the new x -axis, and then the new y -axis, sequentially (for a body facing the positive y -axis). These rotations are called yaw, pitch, and roll, respectively.

Torsional persistence length. The length over which thermal twisting fluctuations become substantial. Typically defined as

the statistical correlation length of relative filament twist at two points along the filament's contour.

Torsional rigidity. The torque required to twist a filament to unit twisting angle.

Wormlike chain. Filament conformation model which assumes that filaments curve and/or twist continuously along their contours.

Zimm model. Filament dynamics model that treats filaments with 'springs and beads', and that assumes strong hydrodynamic interactions between the beads (called the non-draining assumption).

References

- [1] Mogilner A 2006 *Curr. Opin. Cell Biol.* **18** 32
- [2] MacKintosh F C and Janmey P A 1997 *Curr. Opin. Solid State Mater. Sci.* **2** 350
- [3] Palmer J S and Boyce M C 2008 *Acta Biomaterialia* **4** 597
- [4] Ryan G, Watanabe N and Vavylonis D 2012 *Cytoskeleton* **69** 195
- [5] Zhu J and Mogilner A 2012 *PLoS Comput. Biol.* **8** e1002764
- [6] Kolinski A 2011 *Lattice polymers and protein models: Multiscale Approaches to Protein Modeling* 1st edn (New York: Springer)
- [7] Niranjan P S *et al* 2001 *J. Chem. Phys.* **114** 10573
- [8] Dudowicz J, Freed K F and Douglas J F 1999 *J. Chem. Phys.* **111** 7116
- [9] Brion P and Westhof E 1997 *Annu. Rev. Biophys. Biomol. Struct.* **26** 113
- [10] Dobson C M 2003 *Nature* **426** 884
- [11] Alberts B *et al* 2008 *Molecular Biology of the Cell* 5th edn (New York: Garland Science)
- [12] Howard J 2001 *Mechanics of Motor Proteins and the Cytoskeleton* (Sunderland, MA: Sinauer Associates)
- [13] Pollard T D 1986 *Annu. Rev. Biochem.* **55** 987
- [14] Pollard T D and Borisy G G 2003 *Cell* **112** 453
- [15] Nogales E 2000 *Annu. Rev. Biochem.* **69** 277
- [16] Kirschner M and Mitchison T 1986 *Cell* **45** 329
- [17] Herrmann H, Bär H, Kreplak L, Strelkov S V and Aebi U 2007 *Nature Rev. Mol. Cell Biol.* **8** 562
- [18] Møller-Jensen J and Löwe J 2005 *Curr. Opin. Cell Biol.* **17** 75
- [19] Cabean M T and Jacobs-Wagner C 2010 *Annu. Rev. Genet.* **44** 365
- [20] Derman A I *et al* 2009 *Mol. Microbiol.* **73** 534
- [21] Jones L J F, Carballido-López R and Errington J 2001 *Cell* **104** 913
- [22] Wang S, Arellano-Santoyo H, Combs P A and Shaevitz J W 2010 *Proc. Natl Acad. Sci. USA* **107** 9182
- [23] Osteryoung K W and Nunnari J 2003 *Science* **302** 1698
- [24] Vaughan S, Wickstead B, Gull K and Addinall S G 2004 *J. Mol. Evol.* **58** 19
- [25] Erickson H P 2009 *Proc. Natl Acad. Sci. USA* **106** 9238
- [26] Margolin W 2005 *Nature Rev. Mol. Cell Biol.* **6** 862
- [27] Romberg L and Levin P A 2003 *Annu. Rev. Microbiol.* **57** 125
- [28] Ausmees N, Kuhn J R and Jacobs-Wagner C 2003 *Cell* **115** 705
- [29] Trachtenberg S *et al* 2008 *J. Mol. Biol.* **378** 778
- [30] Lutkenhaus J 2012 *Trends Microbiol.* **20** 411
- [31] Lutkenhaus J 2007 *Annu. Rev. Biochem.* **76** 539
- [32] Hagerman P J 1988 *Annu. Rev. Biophys. Biophys. Chem.* **17** 265
- [33] Felsenfeld G and Groudine M 2003 *Nature* **421** 448
- [34] Rajapakse I and Groudine M 2011 *J. Cell Biol.* **192** 711
- [35] Langowski J 2006 *Eur. Phys. J. E* **19** 241
- [36] Marko J F and Siggia E D 1994 *Macromolecules* **27** 981
- [37] Gittes F, Mickey B, Nettleton J and Howard J 1993 *J. Cell Biol.* **120** 923

- [38] Kikumoto M, Kurachi M, Tosa V and Tashiro H 2006 *Biophys. J.* **90** 1687
- [39] Landau L D and Lifshitz E M 1986 *Theory of Elasticity* 3rd edn (Oxford: Elsevier)
- [40] Doi M 1995 *Introduction to Polymer Physics* (Oxford: Oxford University Press)
- [41] Doi M and Edwards S F 1986 *The Theory of Polymer Dynamics* (Oxford: Oxford University Press)
- [42] Yamakawa H 1971 *Modern Theory of Polymer Solutions* (New York: Harper and Row)
- [43] Baumgärtner A 1984 *Annu. Rev. Phys. Chem.* **35** 419
- [44] Kumar S and Li M S 2010 *Phys. Rep.* **486** 1
- [45] Kuhn V W 1934 *Kolloidn. Z.* **68** 2
- [46] Guth E and Mark H 1934 *Monatsh. Chem.* **65** 93
- [47] Smith D E, Perkins T T and Chu S 1996 *Macromolecules* **29** 1372
- [48] Bustamante C, Marko J F, Siggia E D and Smith S 1994 *Science* **265** 1599
- [49] Andrews S S and Arkin A P 2007 *Biophys. J.* **93** 1872
- [50] Klenin K, Merlitz H and Langowski J 1998 *Biophys. J.* **74** 780
- [51] Huang J and Schlick T 2002 *J. Chem. Phys.* **117** 8573
- [52] Chirico G and Langowski J 1996 *Biophys. J.* **71** 955
- [53] Shimada J and Yamakawa H 1984 *Macromolecules* **17** 689
- [54] Goldstein H 1980 *Classical Mechanics* 2nd edn (Reading, MA: Addison-Wesley)
- [55] Hörger I *et al* 2008 *Phys. Rev. E* **77** 011902
- [56] Kratky O and Porod G 1949 *Rec. Trav. Chim. Pays-Bas* **68** 1106
- [57] Yamakawa H 1976 *Pure Appl. Chem.* **46** 135
- [58] Bustamante C, Smith S B, Liphardt J and Smith D 2000 *Curr. Opin. Struct. Biol.* **10** 279
- [59] Marko J F and Siggia E D 1995 *Macromolecules* **28** 8759
- [60] Howard J 2008 *Cell. Mol. Bioeng.* **1** 24
- [61] Yanagida T, Nakase M, Nishiyama K and Oosawa F 1984 *Nature* **307** 58
- [62] Mickey B and Howard J 1995 *J. Cell Biol.* **130** 909
- [63] Mücke N *et al* 2004 *J. Mol. Biol.* **335** 1241
- [64] Kiss B, Karsai Á and Kellermayer M S Z 2006 *J. Struct. Biol.* **155** 327
- [65] Liu X and Pollack G H 2002 *Biophys. J.* **83** 2705
- [66] Smith S B, Finzi L and Bustamante C 1992 *Science* **258** 1122
- [67] Wang M D, Yin H, Landick R, Gelles J and Block S M 1997 *Biophys. J.* **72** 1335
- [68] Käs J *et al* 1996 *Biophys. J.* **70** 609
- [69] Taute K M, Pampaloni F, Frey E and Florin E-L 2008 *Phys. Rev. Lett.* **100** 028102
- [70] Odijk T 1995 *Macromolecules* **28** 7016
- [71] Wiggins P A *et al* 2006 *Nature Nanotechnol.* **1** 137
- [72] Wiggins P A and Nelson P C 2006 *Phys. Rev. E* **73** 031906
- [73] Maier B and Rädler J O 2000 *Macromolecules* **33** 7185
- [74] Schlick T, Beard D A, Huang J, Strahs D A and Qian X 2000 *Comput. Sci. Eng.* **2** 38
- [75] Cloutier T E and Widom J 2005 *Proc. Natl Acad. Sci. USA* **102** 3645
- [76] Turner M S, Briehl R W, Ferrone F A and Josephs R 2003 *Phys. Rev. Lett.* **90** 128103
- [77] Strick T, Allemand J-F, Croquette V and Bensimon D 2000 *Prog. Biophys. Mol. Biol.* **74** 115
- [78] Chelminiak P, Dixon J M and Tuszyński J A 2010 *Eur. Phys. J. E* **31** 215
- [79] Kornberg A and Baker T A 2005 *DNA Replication* 2nd edn (Sausalito, CA: University Science Books)
- [80] Mitchison T and Kirschner M 1984 *Nature* **312** 237
- [81] Howard J and Hyman A A 2003 *Nature* **422** 753
- [82] Gardner M K, Zanic M and Howard J 2013 *Curr. Opin. Cell Biol.* **25** 14
- [83] Tirnauer J S, Salmon E D and Mitchison T J 2004 *Mol. Biol. Cell* **15** 1776
- [84] Carazo-Salas R E, Gruss O J, Mattaj I W and Karsenti E 2001 *Nature Cell Biol.* **3** 228
- [85] Janson M E, Dood M E and Dogterom M 2003 *J. Cell Biol.* **161** 1029
- [86] Pollard T D and Mullins R D 2000 *Annu. Rev. Biomol. Struct.* **29** 545
- [87] Khan S M, Ali R, Asi N and Molloy J E 2012 *Communicative Integrative Biol.* **5** 1
- [88] Fuchs E and Weber K 1994 *Annu. Rev. Biochem.* **63** 345
- [89] Eriksson J E, Opal P and Goldman R D 1992 *Curr. Opin. Cell Biol.* **4** 99
- [90] Godsel L M, Hobbs R P and Green K J 2007 *Trends Cell Biol.* **18** 28
- [91] Shih Y-L and Rothfield L 2006 *Microbiol. Mol. Biol. Rev.* **70** 729
- [92] Erickson H P, Anderson D E and Osawa M 2010 *Microbiol. Mol. Biol. Rev.* **74** 504
- [93] Purcell E M 1977 *Am. J. Phys.* **45** 3
- [94] Fulton A B 1982 *Cell* **30** 345
- [95] Rouse P E J 1953 *J. Chem. Phys.* **21** 1272
- [96] Zimm B H 1956 *J. Chem. Phys.* **24** 269
- [97] De Gennes P G 1974 *J. Chem. Phys.* **60** 5030
- [98] Harnau L, Winkler R G and Reineker P 1996 *J. Chem. Phys.* **104** 6355
- [99] Chirico G and Langowski J 1992 *Macromolecules* **25** 769
- [100] Hagerman P J and Zimm B H 1981 *Biopolymers* **20** 1481
- [101] Broersma S 1960 *J. Chem. Phys.* **32** 1626
- [102] Broersma S 1960 *J. Chem. Phys.* **32** 1632
- [103] Tirado M M, Martínez C L and García de la Torre J 1984 *J. Chem. Phys.* **81** 2047
- [104] Janson M E and Dogterom M 2004 *Biophys. J.* **87** 2723
- [105] Wiggins C H, Rivelino D, Ott A and Goldstein R E 1998 *Biophys. J.* **74** 1043
- [106] Harris R A and Hearst J E 1966 *J. Chem. Phys.* **44** 2595
- [107] Fujime S and Maruyama M 1973 *Macromolecules* **6** 237
- [108] Maeda T and Fujime S 1981 *Macromolecules* **14** 809
- [109] Yamakawa H, Yoshizaki T and Fujii M 1986 *J. Chem. Phys.* **84** 4693
- [110] Fujime S and Maeda T 1985 *Macromolecules* **18** 191
- [111] Pecora R 1991 *Science* **251** 893
- [112] Eimer W and Pecora R 1991 *J. Chem. Phys.* **94** 2324
- [113] Lumma D, Keller S, Vilgis T and Rädler R O 2003 *Phys. Rev. Lett.* **90** 218301
- [114] Winkler R G, Keller S and Rädler J O 2006 *Phys. Rev. E* **73** 041919
- [115] Lukacs G L *et al* 2000 *J. Biol. Chem.* **275** 1625
- [116] Petrov E P, Ohrt T, Winkler R G and Schwille P 2006 *Phys. Rev. Lett.* **97** 258101
- [117] Perkins T T, Quake S R, Smith D E and Chu S 1994 *Science* **264** 822
- [118] Sorlie S S and Pecora R 1990 *Macromolecules* **23** 487
- [119] Frembgen-Kesner T and Elcock A H 2009 *J. Chem. Theory Comput.* **5** 242
- [120] Ando T and Skolnick J 2010 *Proc. Natl Acad. Sci. USA* **107** 18457
- [121] De Gennes P G 1971 *J. Chem. Phys.* **55** 572
- [122] Perkins T T, Smith D E and Chu S 1994 *Science* **264** 819
- [123] Käs J, Strey H and Sackmann E 1994 *Nature* **368** 226
- [124] Alberts J B and Odell G M 2004 *PLoS Biol.* **2** e412
- [125] Kierfeld J, Frentzel K, Kraikivski P and Lipowsky R 2008 *Eur. Phys. J. Spec. Top.* **157** 123
- [126] Lowe C P 2003 *Phil. Trans. R. Soc. Lond. B* **358** 1543
- [127] Huopaniemi I, Luo K, Ala-Nissila T and Ying S-C 2006 *J. Chem. Phys.* **125** 124901
- [128] Press W H, Flanner B P, Teukolsky S A and Vetterling W T 1988 *Numerical Recipes in C* (Cambridge: Cambridge University Press)
- [129] Liu C and Muthakumar M 1988 *J. Chem. Phys.* **109** 2536

- [130] Channels W E and Iglesias P A 2010 Simulating filament dynamics in cellular systems *Elements of Computational Systems Biology* ed H M Lodhi and S H Muggleton (Hoboken, NJ: Wiley)
- [131] Nédélec F and Foethke D 2007 *New J. Phys.* **9** 427
- [132] Alberts J B 2009 *PLoS One* **4** e4748
- [133] Rafelski S M, Alberts J B and Odell G M 2009 *PLoS Comput. Biol.* **5** e1000434
- [134] Mincer J S and Simon S M 2011 *Proc. Natl Acad. Sci. USA* **108** E351
- [135] Zimmerman S B and Minton A P 1993 *Annu. Rev. Biophys. Biomol. Struct.* **22** 27
- [136] Andrews S S 2004 *J. Chem. Educ.* **81** 877
- [137] Horowitz D S and Wang J C 1984 *J. Mol. Biol.* **173** 75
- [138] Bensimon D, Simon A J, Croquette V and Bensimon A 1995 *Phys. Rev. Lett.* **74** 4754
- [139] Tsuda Y, Yasutake H, Ishijima A and Yanagida T 1996 *Proc. Natl Acad. Sci. USA* **93** 12937
- [140] Carballido-López R 2006 *Microbiol. Mol. Biol. Rev.* **70** 888
- [141] Chrétien D and Wade R H 1991 *Biol. Cell* **71** 161
- [142] Janson M E and Dogterom M 2004 *Biophys. J.* **87** 2723
- [143] Larsen R A *et al* 2007 *Genes Dev.* **21** 1340
- [144] Kreplak L and Fudge D 2007 *Bioessays* **29** 26